Supplmentary Material for "Superconducting and Antiferromagnetic Properties of Dual-Phase V_3Ga"

Michelle E. Jamer,[1] Brandon Wilfong,[1] Vasiliy D. Buchelnikov,[2,3] Vladimir V. Sokolovskiy,[2,3] Olga N. Miroshkina,[2,4] Mikhail A. Zagrebin,[2,3,5] Danil R. Baigutlin,[2,4] Jared Naphy,[1] Badih A. Assaf,[6] Laura H. Lewis,[7] Aki Pulkkinen,[8,4] Bernardo Barbiellini,[4,9] Arun Bansil,[9] and Don Heiman[9]

[1)] *Physics Department, United States Naval Academy, Annapolis, MD 20899, USA*

[2)] *Faculty of Physics, Chelyabinsk State University, 454001 Chelyabinsk, Russia*

[3)] *National University of Science and Technology "MISiS", 119049 Moscow, Russia*

[4)] *Department of Physics, School of Engineering Science, LUT University, FI-53850 Lappeenranta, Finland*

[5)] *National Research South Ural State University, 454080 Chelyabinsk, Russia*

[6)] *Physics Department, University of Notre Dame, South Bend, IN 46556, USA*

[7)] *Chemical Engineering Department, Northeastern University, Boston, MA 02115, USA*

[8)] *Département de Physique and Fribourg Center for Nanomaterials, Université de Fribourg, CH-1700 Fribourg, Switzerland*

[9)] *Physics Department, Northeastern University, Boston, MA 02115, USA*

(Dated: 20 July 2020)

1. Details and Results of the VASP calculations

The geometric optimization and ground state calculations were performed for two structures ($D0_3$ and β-W A15) of V_3Ga, which are experimentally observed. In the case of the $D0_3$ structure, the 16-atom supercell was considered in which Ga atoms locate at $4a$ (0.0, 0.0, 0.0) Wyckoff positions and V atoms occupy $4b$ (1/2, 1/2, 1/2) and $8c$ ((1/4, 1/4, 1/4) and 3/4, 3/4, 3/4)) sites. For the A15 structure, a six-atom supercell was used in which the two Ga atoms occupy the $2a$ sites and the six V atoms locate at $6c$ sites. Concerning the magnetic subsystem, ferromagnetic (FM) and antiferromagnetic (AFM) spin alignments of V atoms were considered. For the $D0_3$ structure, FM and AFM G-type orders were considered along the lines Ref.[1], while for the A15 structure, FM and three AFM orders were computed as suggested in Ref.[2]. The crystal structures and magnetic configurations considered are illustrated in Fig. S1. In order to emphasize the AFM state, V atoms located at different sites are labelled as 1, 2, and 3.

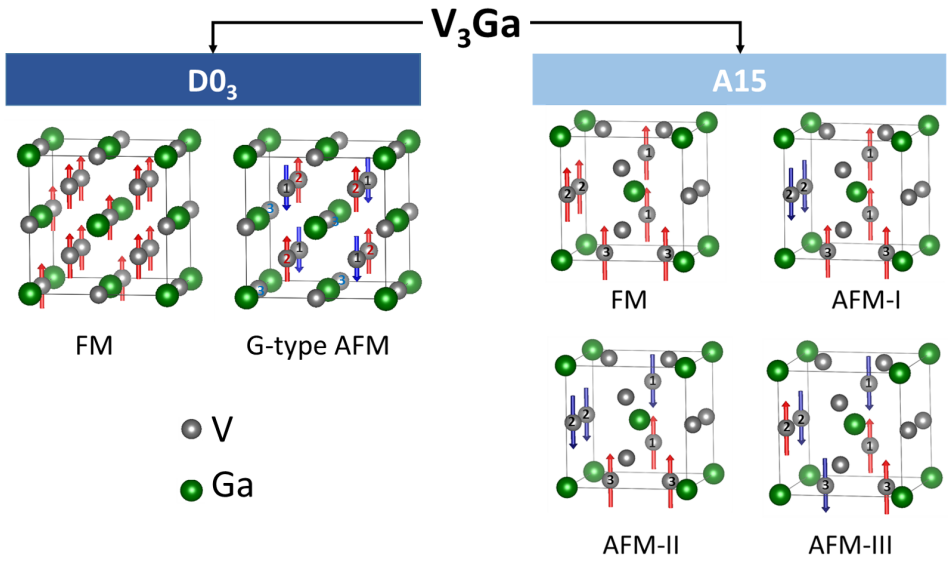

FIG. S1. Various magnetic ordering of $D0_3$ and A15 structures of V_3Ga on which computations were carried out. V atoms located at different sites are labelled 1, 2, and 3.

In order to understand the robustness of our results we carried out computations using four different schemes for treating exchange-correlation effects: LDA-PZ[3], GGA-PBE[4–6], GGA+U and meta-GGA-SCAN[7–9]. For the GGA+U

scheme, the values of Hubbard-repulsion U and Hund-exchange integral J for the V atoms were taken to be 2 eV and 0.67 eV, respectively following He *et al.*[2]. The PAW-pseudopotentials were taken with valence-electron configurations as follows: $3s^2 3p^6 4s^2 3d^3$ for V atoms and $3d^{10} 4s^2 4p^1$ for Ga atoms. The 10×10×10 k-point-grid used in the computations was generated using via the Monkhorst-Pack scheme. The kinetic-energy cutoff for the augmented plain waves was taken to be 750 eV. The Methfessel-Paxton smearing method[10] was used with a width of 0.2 eV in geometry optimization runs, and the tetrahedron smearing method with Blóchl corrections[11] was deployed in self-consistent calculations. Total energies were converged to an accuracy of 10^{-8} eV. The convergence criterion in the optimization for the residual forces was 10^{-7} eV/Å. Results for the $D0_3$ and A15 structures of V_3Ga are presented in Tables S1 and S2.

TABLE S1. Equilibrium lattice parameter (a_0 in Å), partial and total magnetic moments (μ_{V_i} and μ_{tot} in μ_B/f.u.), and total energies (E in eV/atom) of non-magnetic (NM) and AFM phases of $D0_3$ structure. Notice, the initial FM order was converged to the non-magnetic (NM) one.

	NM					
	a_0	μ_{V_1}	μ_{V_2}	μ_{V_3}	μ_{tot}	E
LDA	5.899	0.00	0.00	0.00	0.00	-8.486
PBE	6.034	0.00	0.00	0.00	0.00	-7.574
PBE+U	6.059	0.00	0.00	0.00	0.00	-6.541
SCAN	5.977	0.00	0.00	0.00	0.00	-17.377
	AFM					
	a_0	μ_{V_1}	μ_{V_2}	μ_{V_3}	μ_{tot}	E
LDA	5.902	-0.429	0.429	0.00	0.00	-8.487
PBE	6.064	-1.314	1.314	0.00	0.00	-7.600
PBE+U	6.130	-1.916	1.916	0.00	0.00	-6.647
SCAN	6.035	-1.848	0.00	1.848	0.00	-17.486

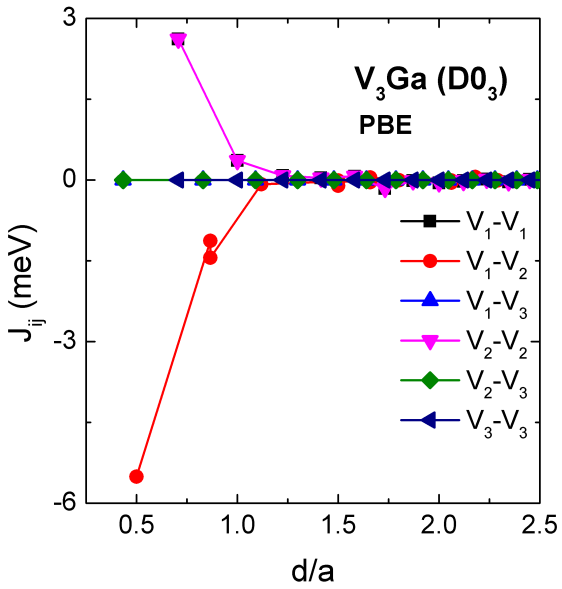

FIG. S2. Exchange coupling constants J_{ij} as a function of the distance (d/a) between the atoms i and j in the V_3Ga with $D0_3$ structure at the equilibrium lattice parameter

2. Details and Results of the SPR-KKR calculations

The Heisenberg exchange-coupling parameters (J_{ij}) were obtained by using the spin-polarized scalar-relativistic (SPSREL) Dirac-Hamiltonian as part of the SPR-KKR (spin-polarized relativistic Korringa-Kohn-Rostoker) package[12].

TABLE S2. The equilibrium lattice parameter (a_0 in Å), partial and total magnetic moments (μ_{V_i} and μ_{tot} in μ_B/f.u.), and total energy (E in eV/atom) of FM and AFM phases of A15 structure.

			FM			
	a_0	μ_{V_1}	μ_{V_2}	μ_{V_3}	μ_{tot}	E
LDA	4.678	0.089	0.164	0.112	0.368	-8.572
PBE	4.788	0.222	0.390	0.303	0.916	-7.645
PBE+U	4.817	0.434	0.661	0.548	1.636	-6.601
SCAN	4.744	0.308	0.523	0.414	1.244	-17.442
			AFM-I			
	a_0	μ_{V_1}	μ_{V_2}	μ_{V_3}	μ_{tot}	E
LDA	4.678	0.097	0.122	0.147	0.368	-8.572
PBE	4.788	0.248	0.306	0.361	0.916	-7.645
PBE+U	4.828	0.576	0.307	0.760	1.636	-6.602
SCAN	4.742	0.00	0.00	0.00	0.00	-17.436
			AFM-II			
	a_0	μ_{V_1}	μ_{V_2}	μ_{V_3}	μ_{tot}	E
LDA	4.677	0.00	0.00	0.00	0.00	-8.572
PBE	4.786	0.00	0.00	0.00	0.00	-7.643
PBE+U	4.801	±1.036	±0.024	±0.007	0.00	-6.594
SCAN	4.742	±0.355	±0.002	±0.017	0.00	-17.436
			AFM-III			
	a_0	μ_{V_1}	μ_{V_2}	μ_{V_3}	μ_{tot}	E
LDA	4.678	0.00	0.00	0.00	0.00	-8.572
PBE	4.788	0.00	0.00	0.00	0.00	-7.643
PBE+U	4.879	±1.351	±1.508	±1.502	0.00	-6.632
SCAN	4.744	±0.268	±0.326	±0.330	0.00	-17.437

For these calculations, the optimized lattice parameter was obtained by a VASP-based calculation for the FM phase of $D0_3$ structure. Here, calculations were carried out for a unit cell of $D0_3$ consisting of four atoms (3 V and 1 Ga). The exchange-correlation energy was treated by the GGA-PBE parameterization[5]. For the self-consistency cycles, 2300 k-points were generated by a k-mesh grid of 45^3. The angular momentum expansion (l_{max})was restricted to three. The magnetic exchange constants were calculated on a k-mesh grid of $57 \times 57 \times 57$ with 4495 k-points. All calculations converged to 0.01 mRy for total energy. Dependence of the exchange-interaction parameters J_{ij} on the distance between the atoms d/a is shown in Fig. S2.

Here, the positive exchange constants ($J_{ij} > 0$) imply FM coupling, whereas negative values ($J_{ij} < 0$) indicate AFM coupling. Large FM interactions are seen between the nearest neighbor V_1-V_1 and V_2-V_2 atoms. Magnitudes of both these couplings are about of 3 meV. The couplings are zero in the third and farther coordination shells. The strongest AFM interaction (-5.5 meV) occurs between the nearest V_1 and V_2 atoms in different sublattices. All interactions with V_3 atoms are close to zero (Table 1).

3. Details and Results of the Monte Carlo simulations

To extend the zero-temperature *ab initio* results to finite temperatures, we further performed Monte Carlo (MC) simulations on the classical three-dimensional Heisenberg model ($\mathcal{H} = \mathrm{fl} \sum_{ij} J_{ij} S_i S_j$) in zero magnetic field. Here, $\mathbf{S}_i = (S_i^x,\ S_i^y,\ S_i^z)$ is a classical Heisenberg spin variable $|S_i| = 1$ and J_{ij} are the exchange-coupling constants (positive for FM and negative for AFM interactions). The calculated exchange parameters (J_{ij}) and partial magnetic moments (μ_i) were taken as input parameters. Values of J_{ij}'s show long-range oscillations as a function of the distance between the atoms (d/a). We restricted exchange interactions up to the sixth coordination shell for all interaction pairs.

The MC simulations were carried out for a lattice with a unit cell consisting of 3925 atoms (1099 Ga and 2826 V atoms) with periodic boundary conditions. The Metropolis algorithm[13] was used where a new, random spin direction was chosen and the resulting energy change was calculated. Changes in the independent spin variables $\mathbf{S}_i = (S_i^x,\ S_i^y,\ S_i^z)$ were accepted or rejected based on the single-site transition probability $W = \min\left[1, \exp\left(-\Delta\mathcal{H}/k_B T\right)\right]$. As the time step, we used one MC step consisting of N attempts to change the spin variables. A new spin direction can be chosen by randomly choosing new spin components. The spin components were chosen in the following manner[13]. Two random numbers r_1 and r_2 are chosen from the interval $[0, 1]$ to produce a vector with two components $\zeta_1 = 1 - 2r_1$

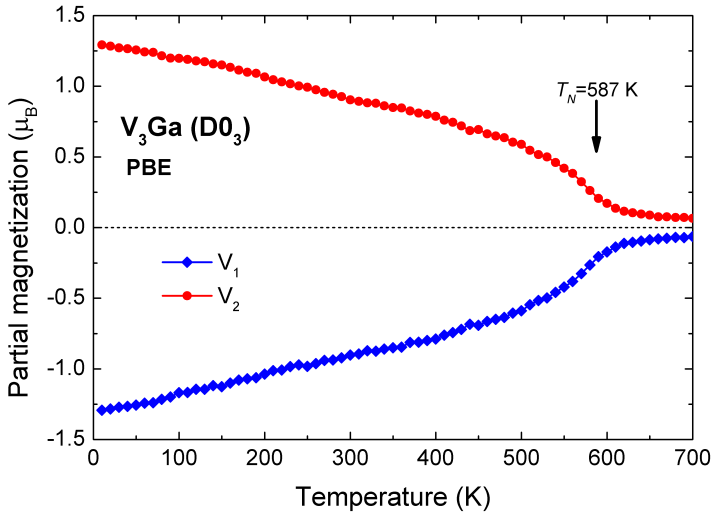

FIG. S3. Temperature variation of the partial magnetization curves for V_3Ga in the $D0_3$ structure at zero magnetic field.

and $\zeta_2 = 1-2r_2$. Length of the vector is determined by $\zeta^2 = \zeta_1^2+\zeta_2^2$ and if $\zeta^2 < 1$, then a new spin vector is computed with components

$$S_i^x = 2\zeta_1\sqrt{1-\zeta^2},\ S_i^y = 2\zeta_2\sqrt{1-\zeta^2},\ S_i^z = 1-2\zeta^2.$$

At each temperature properties (internal energy of the system $\langle\mathcal{H}\rangle$ and magnetic order parameter $\langle m\rangle$) were estimated allowing 10^5 MC steps and 10^4 thermalization steps and were averaged over 2250 configurations for each 400 MC steps. The simulation started from the ferromagnetic phase with $S_i^z = 1$.

The magnetic order parameter is defined as follows:

$$m^\alpha = \frac{1}{N^\alpha}\sum_i \sqrt{\left(S_i^{\alpha,x}\right)^2 + \left(S_i^{\alpha,y}\right)^2 + \left(S_i^{\alpha,z}\right)^2},$$

where α denotes the V_1, V_2 and V_3 atoms and N^α the total number of α atoms; i runs over the corresponding lattice sites of the α atoms. The resulting temperature dependencies of partial magnetizations of $V_{1,2}$ for V_3Ga with $D0_3$ alloy at zero magnetic field is shown in Fig. S3.

In order to estimate the Neél temperature, we plotted $m\,(T) = \left(m^\alpha\right)^{1/\beta}(T)$ function, which approximately decreases linearly with increasing temperature. The Neél temperature can then be estimated from the intersection of m with the T axis. Here, m^α is the partial magnetization of V_1 and V_2 atoms and β is the critical index. Note, in the case of the three-dimensional Heisenberg model the β exponent is equal to 0.3646. In this way, we obtain the estimated Neél temperature $T_N = 587$ K.

4. Results of Disorder Calculations

Effects of disorder on the Neél temperature were obtained using the SPR-KKR package based on the KKR-CPA approach. The degree of disorder in the atomic sublattices was quantified by x, which is defined as the fraction of Ga atoms that are exchanged for nonmagnetic V atoms (V_3), where the nonmagnetic V atoms lie between the two antiferromagnetically coupled magnetic V atoms (V_1 and V_2). Results are given in Table S3 for $x = 0$ to 0.2. For all values of x, the V_1 and V_2 magnetic atoms have opposite orientation and equal magnetic moments, while the V_3 moment is zero.

Calculated magnetic exchange-coupling parameters (J_{ij}) for the $D0_3$ phase for various degrees of disorder x are presented in Fig. S4. Dominant exchange interactions, FM V_1-V_3 and V_2-V_2, and AFM V_1-V_2, weaken substantially with increasing disorder. For $x = 0.2$, all J_{ij} are almost zero (Fig. S4(b)). These results suggest that the Neél temperature will decrease with rising disorder. Mean-field calculations using these J_{ij}'s show a decrease in the Neél

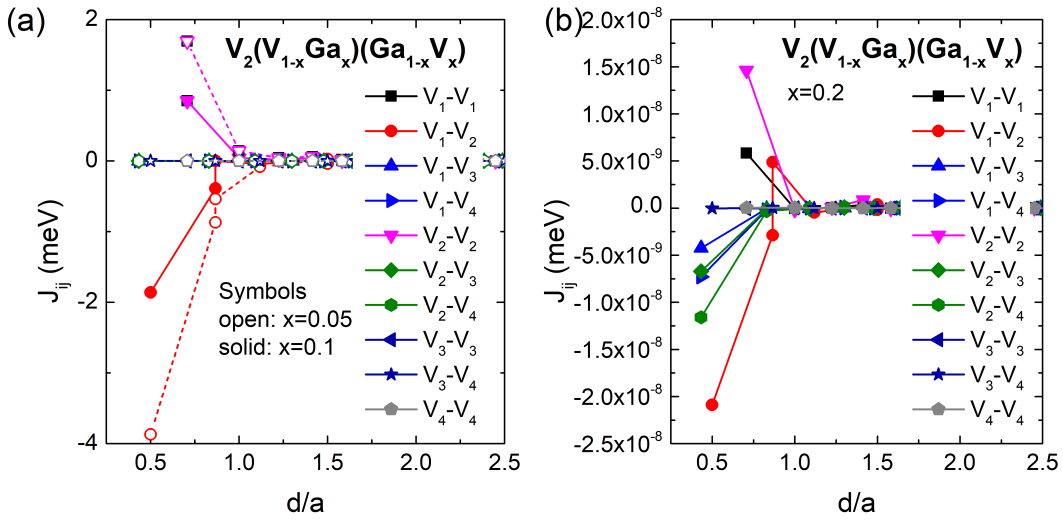

FIG. S4. Exchange coupling constants J_{ij} as a function of the distance (d/a) between the atoms i and j for $D0_3$ phase of V_3Ga for several different values of disorder x.

TABLE S3. Partial magnetic moments of V_i atoms and the Neél temperatures calculated for $D0_3$ phase of V_3Ga for different degrees of disorder x. Note, that $x = 0$ refers to the ordered $D0_3$ structure.

Degree of disorder	μ_{V_1}	μ_{V_2}	μ_{V_3}	μ_{V_4}	μ_{tot}	T_N
0	-1.161	1.161	0.00	-	0.00	630.0
0.05	-0.997	0.997	0.00	0.00	0.00	414.5
0.1	-0.720	0.720	0.00	0.00	0.00	189.3
0.2	0.002	0.002	0.00	0.00	0.00	0.00

temperature from $T_N = 630$ K at $x = 0$ to $T_N = 0$ K at $x = 0.2$ (Table S3). We would expect a similar behavior from Monte Carlo simulations.

5. Results of Rietveld X-ray diffraction analysis

X-ray diffraction from the V_3Ga sample was taken at Beamline 11-BM at the Advanced Photon Source at Argonne National Lab using a wavelength of $\lambda = 0.413841$ Å. The sample was rotated continuously. Fig. S5 shows the XRD data and the results of the subsequent Rietveld and Pawley fitting procedures.[14] The experimental data is shown by points and the fit is shown by the pink curve. The lower blue curve plots the experimental data minus the Rietveld fit. Here, only the A15, $D0_3$ and A2 phases were included in the Rietveld fitting procedure. The A2 phase is a disordered $D0_3$ phase where the V and Ga atoms are randomly exchanged. When we included only these three phases, our analysis indicated that there was still another missing phase. A search of relevant V, Ga and V-Ga binary phases (V_6Ga5, V_6Ga_7, V_2Ga_5) were unable to accurately index the remaining peaks. Thus, an expanded search to contain impurity oxide phases was done. In this way, we determined that the remaining peaks could be accurately indexed to the reported oxide impurity phase, V_3GaO_x.[15] The structure of the V_3GaO_x phase has not been rigorously reported; however, the previous work has discussed the structure as Cu_3Au-type perovskite with Ga at the corners, V at the face centers and O at the body center. From this, a structure was built and the space group determined through the use of the Python Materials Genomics library.[16] Since the structure of the V_3GaO_x has not been determined and its existence as a minor impurity phase has not been clearly established in the current work, it's contribution to the X-ray diffraction pattern was modeled only by a Pawley refinement procedure. As such, the weight fraction of the V_3GaO_x phase could not be determined and, therefore, all weight fractions for the A15, $D0_3$, and A2 phases are reported relative to each other. The results of the fitting procedure provided the following approximate percentages of the various phases: 81% in the A15 phase, 18% in the $D0_3$ phase, and 0.1% in the A2 phase. An attempt to include the assumed structure for the V_3GaO_x phase for Rietveld refinement yielded an approximate weight fraction on the order of 30 - 40%.

6. Analysis of superconductivity of the A15 phase

Additional analysis of the as-synthesized superconducting properties of A15 V_3Ga revealed a superconducting critical temperature of 13.6 K and a superconducting volume fraction at 2 K of approximately 90% as shown in

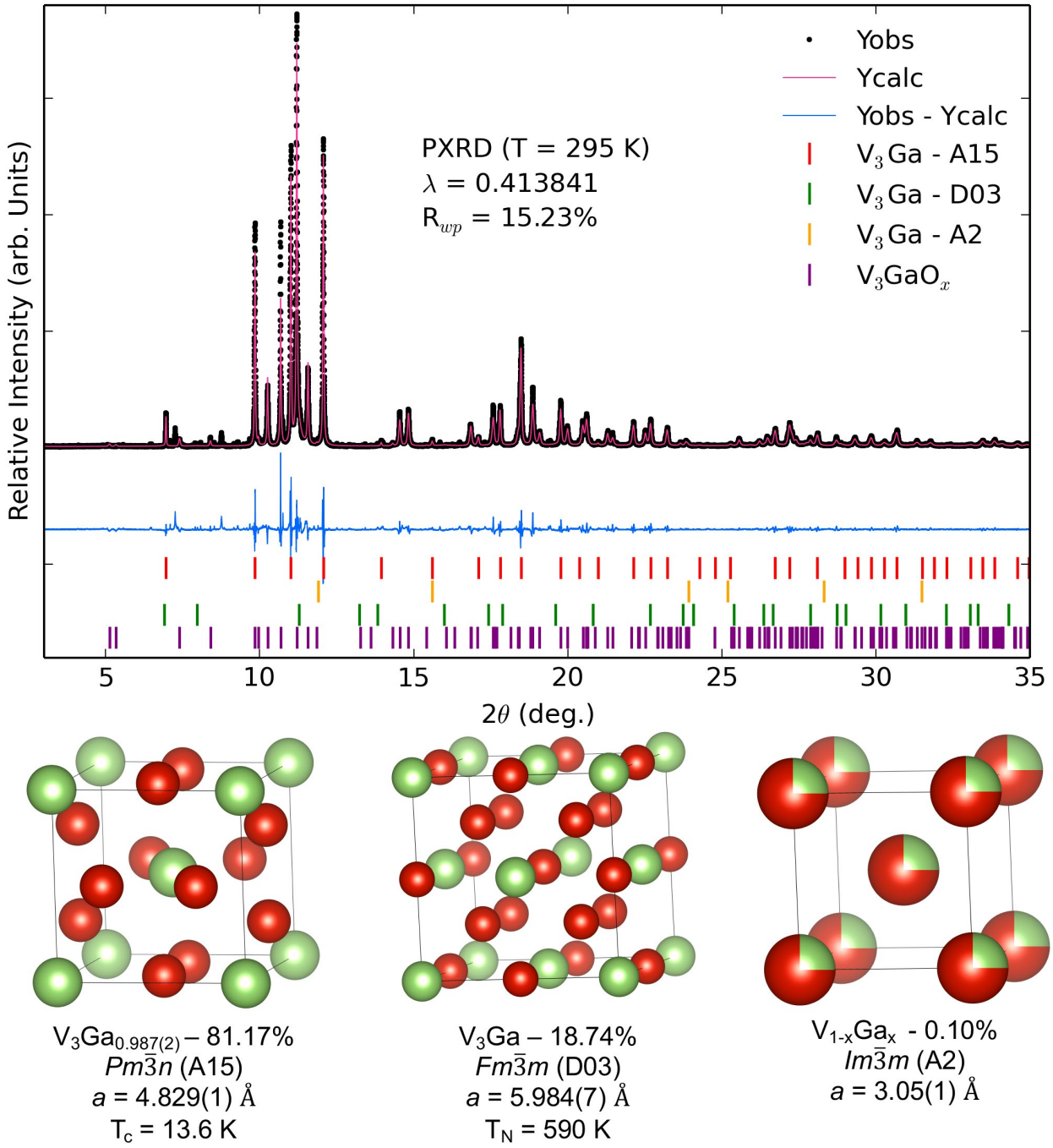

FIG. S5. High resolution synchrotron X-ray diffraction patterns for the as-grown V_3Ga ingots collected at T = 295 K. Red and green tick marks represent the targeted V_3Ga , A15 and $D0_3$ phases respectively. Orange tick marks represent impurity A2 phase and purple tick marks show the existence of an impurity oxide phase, V_3GaO_x. Also shown are the calculated, observed, and differences curves from Rietveld analysis. Crystal structures, the corresponding extracted lattice parameters and the elemental composition from Rietveld analysis, and the relevant transition temperature for each phase are shown below the XRD data.

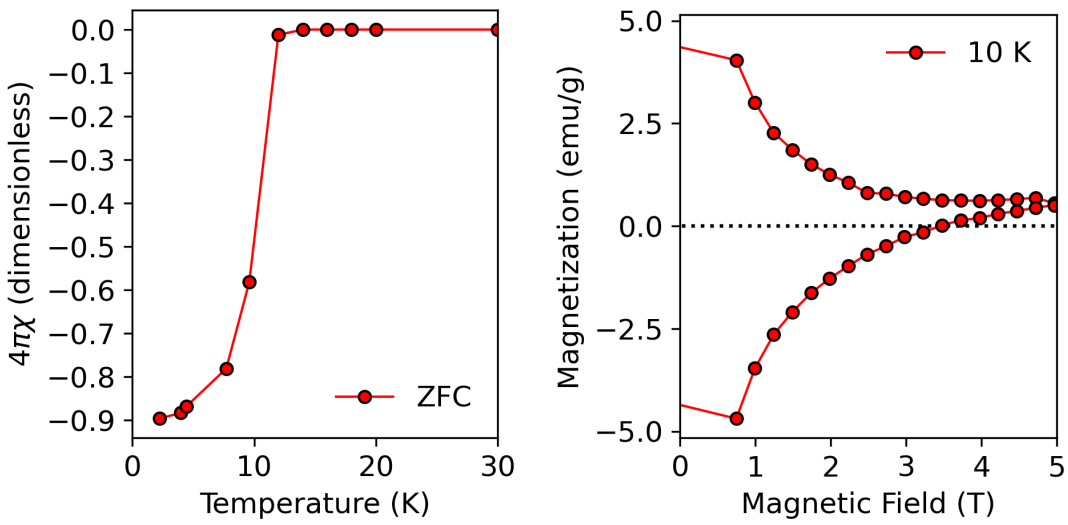

FIG. S6. Temperature dependence of the dimensionless magnetic susceptibility at 0.05 T and the isothermal magnetization at 10 K of the V_3Ga sample mixture measured on the as-synthesized polycrystalline material.

Fig. S6. This was calculated from the density and phase fraction extracted from Rietveld analysis from synchrotron X-ray diffraction data for the A15 phase. Isothermal magnetization at 10 K revealed an upper critical field, H_{c2} of about 3.5 T which is significantly lower than previous reports.[17,18] This is mainly due to the lower Tc of our sample, but could also be affected by a number of factors such as stoichiometric changes in the as-synthesized A15 V_3Ga phase as well as the coexistence of another magnetic phase due to the V_3Ga $D0_3$ phase in the as-synthesized sample. Thus, the assignment of an H_{c2} value to the A15 V_3Ga phase cannot be done in a rigorous way. However, the extracted superconducting volume fraction and superconducting critical temperature matches with expectations.

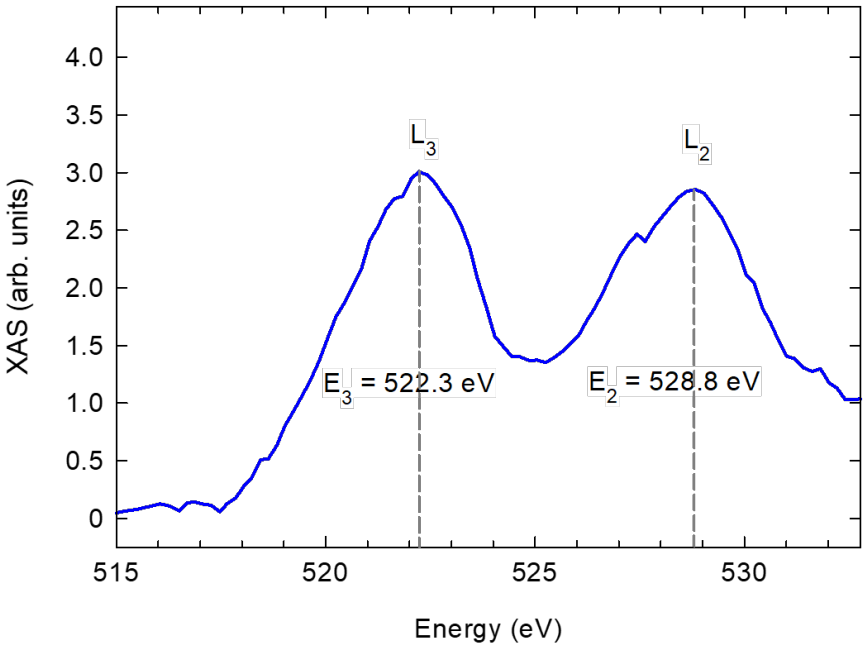

FIG. S7. X-ray absorption spectra at the vanadium L-edge from the V_3Ga ingots collected at 89 K. The L_3 and L_2 edges are marked.

7. X-ray Absorption Spectrum (XAS)

X-ray absorption spectra (XAS) at the vanadium L_3 and L_2 edges were taken using the U4B beamline at the National Synchrotron Light Source at Brookhaven National Laboratory in the total-electron-yield (TEY) mode. The field-dependent measurements were taken at various energies, including energies above, below and at the L_2 and L_3 edges of the V atoms. X-ray magnetic circular dichroism (XMCD) of the V_3Ga ingot was also taken but there was no detectable signal (<0.01%) when comparing data obtained using right- and left-circular polarizations of radiation, and using the complementary technique of changing magnetic field direction. In Fig. S7, the L_3 and L_2 edges are marked. The XAS and XMCD spectra were taken at temperatures between 12.5 K and 300 K, both below and above the superconducting transition, and no ferromagnetic signal was detected.

[1]I. Galanakis, S. Tirpanci, K. Özdoğan, and E. Şaşıoğlu, Phys. Rev. B **94**, 064401 (2016).
[2]B. He et al., Phys. Stat. Sol. (RRL) **13**, 1900483 (2019).
[3]J. P. Perdew and A. Zunger, Phys. Rev. B **23**, 5048 (1981).
[4]J. Perdew, Physica B: Conds. Mater. **172**, 1 (1991).
[5]K. Burke, J. Perdew, and M. Ernzerhof, Int. J. Quant. Chem. **61**, 287 (1997).
[6]J. Perdew, K. Burke, and M. Ernzerhof, Phys. Rev. Lett. **77**, 3865 (1996).
[7]J. P. Perdew, S. Kurth, A. c. v. Zupan, and P. Blaha, Phys. Rev. Lett. **82**, 2544 (1999).
[8]J. Tao, J. P. Perdew, V. N. Staroverov, and G. E. Scuseria, Phys. Rev. Lett. **91**, 146401 (2003).
[9]J. Sun, A. Ruzsinszky, and J. P. Perdew, Phys. Rev. Lett. **115**, 036402 (2015).
[10]M. Methfessel and A. T. Paxton, Phys. Rev. B **40**, 3616 (1989).
[11]P. E. Blöchl, O. Jepsen, and O. K. Andersen, Phys. Rev. B **49**, 16223 (1994).
[12]H. Ebert, D. Ködderitzsch, and J. Minár, Repts. Prog. Phys. **74**, 096501 (2011).
[13]D. P. Landau and K. Binder, A Guide to Monte Carlo Simulations in Statistical Physics, Cambridge University Press, 2 edition, 2005.
[14]A. A. Coelho, J. Appl. Crystallogr. **51**, 210 (2018).
[15]R. Maier, Y. Uzel, and H. Kandler, Zeitschrift für Naturforschung A **21**, 531 (1966).
[16]S. P. Ong et al., Computational Materials Science **68**, 314 (2013).
[17]S. Foner, E. McNiff Jr, S. Moehlecke, and A. Sweedler, Sol. State Commun **39**, 773 (1981).
[18]D. Decker and H. Laquer, J. Appl. Phys. **40**, 2817 (1969).